ARTICLE

Supporting Information

Plasmonic Nanoprism Enhanced Quasi-2D Ruddlesden-Popper Layered Perovskite Photodetectors

Ting Ji [a], Hengkang Zhang [a], Na Han [a], Wenyan Wang [a], Bo Wu [b], Guohui Li [a], Mingming Fan [a], Zhanfeng Li [a], Yuying Hao [a], Furong Zhu [c], Yucheng Wu [a,], and Yanxia Cui [a,]**

a. College of Physics and Optoelectronics, Key Laboratory of Interface Science and Engineering in Advanced Materials, Taiyuan University of Technology, Taiyuan 030024, China
b. Key Laboratory of Flexible Electronics (KLOFE) & Institute of Advanced Materials (IAM), Nanjing Tech University, 30 South Puzhu Road, Nanjing, 211816, China
c. Department of Physics, Institute of Advanced Materials, And Institute of Research and Continuing Education (Shenzhen), Hong Kong Baptist University, Kowloon Tong, Hong Kong, China.
**Corresponding author: yanxiacui@gmail.com (Y. Cui); wyc@tyut.edu.cn (Y. Wu)*

Experimental details

Prepartion of AuAg-NPrisms@SiO_2 solution

First, Ag-NPrisms are synthesized by the seed-mediated approach. The aqueous trisodium citrate (0.25 mL, 500 mg/L), aqueous poly (sodium styrenesulphonate) (PSSS; 0.25 mL, 500 mg/L) and aqueous $NaBH_4$ (0.3 mL, 10 mM) are mixed together in a beaker with continuous stirring. Then the aqueous $AgNO_3$ (5 mL, 0.5 mM) is injected into the above mixed solution at a rate of 2 mL/min with vigorous stirring for 20 min. During the reaction, the color of the mixed solution slowly changes from colorless to brownish, indicating that the seeds solution has been prepared successfully. The second step is to prepare the AuAg-NPrisms based on the above seed solution. Ascorbic acid (75 μL, 10 mM) is diluted with 5 mL distilled water and then added with 100 μL seed solution, which is followed by the injection of $AgNO_3$ (3 mL 0.5 mM) solution at a rate of 1 mL/min with continued stirring for 3 min. The synthesis of Ag NPrisms is finished. In the next step the galvanic replacement approach is adopted to turn Ag NPrisms into AuAg-NPrisms. Ascorbic acid (400 μL, 10 mM) is added into the prepared Ag NPrisms solution, followed by the injection of $HAuCl_4$ (4 mL, 0.5 mM) at a rate of 1 mL/min. 5 min later the AuAg-NPrisms are formed in aqueous solution. In the last step, the AuAg-NPrisms are coated with the tetraethyl orthosilicate (TEOS) in ethanol solution in an alkaline environment and vigorous stirring is continued for 24 h. So far, the synthesis of AuAg-NPrisms@SiO_2 is finished. In order to spin-coat the AuAg-NPrisms@SiO_2 on top of the poly(3,4-ethylenedioxythiophene):polystyrenesulfonate) (PEDOT:PSS) layer without dissolving the underlying PEDOT:PSS layer, it is necessary to change the solution to ethanol by twice centrifugation (7000 rpm, 20 min).

Fabrication of Quasi-2D perovskite photodetectors

The ITO glass substrate is cleaned sequentially in detergent, deionized water, isopropanol, and acetone. Then the PEDOT:PSS layer is spin-coated onto the ITO glass substrates at 7000 rpm for 30 s in air and the sample is annealed on a hot plate at 125 °C for 15 min. Subsequently, the synthesized AuAg-NPrisms@SiO_2 solution at different concentrations is span coated on the top of the PEDOT:PSS layer at 2000 rpm/min for 30 s and then the sample was annealed at 120°C for 10 min. Next, the quasi-2D perovskite $(PEA)_2(MA)_2Pb_3I_{10}$ (PEA = $C_6H_5(CH_2)_2NH_3^+$) solution is spin-coated at 2000 rpm for 45 s and annealed on a hot plate at 70 °C for 10 min under the sec-butyl alcohol environment in a nitrogen glovebox. Here, the $(PEA)_2(MA)_2Pb_3I_{10}$ solution is prepared by mixing No. 1 solution with No. 2 solution by a volume ratio of 2:1, where No. 1 solution was prepared by dissolving 159 mg MAI and 461 mg PbI_2 in a 2 mL anhydrous dimethylformamide (DMF) solvent and No. 2 solution was prepared by dissolving 498 mg PEAI and 461 mg PbI_2 in a 2 mL DMF solvent. In the following, the PCBM solution is spin-coated at 2700 rpm for 30 s to collect electrons efficiently and then poly[(9,9-bis (3'-(*N*, *N*-dimenthylamino)propyl)-2,7-fluorene)-alt-2,7-(9,9-dioctyfluorene)] (PFN) is spin-coated at 7000 rpm for 30 s to reduce the dark current. Finally, a 100 nm silver electrode is deposited by thermal evaporation. The active area of each fabricated quasi-2D PSC device was about 0.04 cm^2, determined by the overlap of the ITO anode and Ag cathode.

Simulation Methods

The simulated configuration is ITO (100 nm)/PEDOT:PSS (30 nm)/$(PEA)_2(MA)_2Pb_3I_{10}$ (60 nm), and the electric field distribution at 565 nm is investigated theoretically by the three-dimensional (3D) Finite Element Method (FEM). The simulation was carried out assuming a periodic boundary along the *x*-axis and *y*-axis, which is normal to the film plane. Perfectly matched layer (PML) boundaries are applied at two planes parallel to the *x*-*y* plane, one lies in the glass and the other is in the air region next to the $(PEA)_2(MA)_2Pb_3I_{10}$ layer. Light is illuminated from the ITO glass side. The wavelength dependent refractive indices and extinction coefficients of the $(PEA)_2(MA)_2Pb_3I_{10}$ are measured in experiment. The refractive indices and extinction coefficients of other materials used in this work are extracted from Refs. [1, 2].

Calculation of hole and electron mobilites

The charge transport was analyzed using space-charge limited current (SCLC) model. The single hole and single electron devices with architectures of ITO/PEDOT:PSS/$(PEA)_2(MA)_2Pb_3I_{10}$/MoO_3/Ag and ITO/$PC_{61}BM$/$(PEA)_2(MA)_2Pb_3I_{10}$/$PC_{61}BM$/PFN/Ag were fabricated with and without 0.7 mM/mL AuAgNPrisms@SiO_2. According to Mott-Gurney law, by assuming the mobility is almost field independent, the relationship between *J* and *V* is obtained, as equation below.

$$J = \frac{9}{8}\varepsilon_r\varepsilon_0\mu\frac{V^2}{d^3},$$

where $\varepsilon_r\varepsilon_0$ is the dielectric constant of the quasi-2D perovskite active layer, d is the thickness of active layer and μ is the carrier mobility. Here ε_r is measured to be about 4.6, d is 60 nm. From the slope of $J^{1/2}$-V curves, hole and electron mobilities are obtained.

Stability of the quasi-2D perovskite PDs

As shown in Fig. S5, the dark current densities of the control and optimal devices at bias voltage of -1 V maintain their original values in the first 240 h and then increase in the next following 240 h. The dark current stability of the optimal device is better than that of the control device. It reflects that incorporation of AuAg-NPrisms@SiO_2 can improve the stability of the quasi-2D $(PEA)_2(MA)_2Pb_3I_{10}$ perovskite PDs, which is due to the crystallinity improvement of the quasi-2D perovskite layer, as shown in Fig.5(a).

Response time of the quasi-2D perovskite PDs

The response time was measured by the transient photocurrent method. A short pulse of light (femtosecond laser) was used to generate photocarriers in the PDs and then the carriers were collected at the electrodes. A fast oscilloscope was used to record the photocurrent pulse. As derived from Fig. S7(a) and (b), the rise and fall times for the control device are 45 and 64 ns, for the optimal device are 29 and 152 ns, respectively, which are among one of the fast response speed PDs due to the vertical structure as well as the thin 2D perovskite active layer (60 nm). Incorporation of AuAg-NPrisms@SiO_2 makes the fall time longer. One can also observe from Table I that the response speed of our devices is the fastest among the reported 2D perovskite PDs. Nevertheless, we believe the response speed can be further improved if each layer of the PDs is optimized.

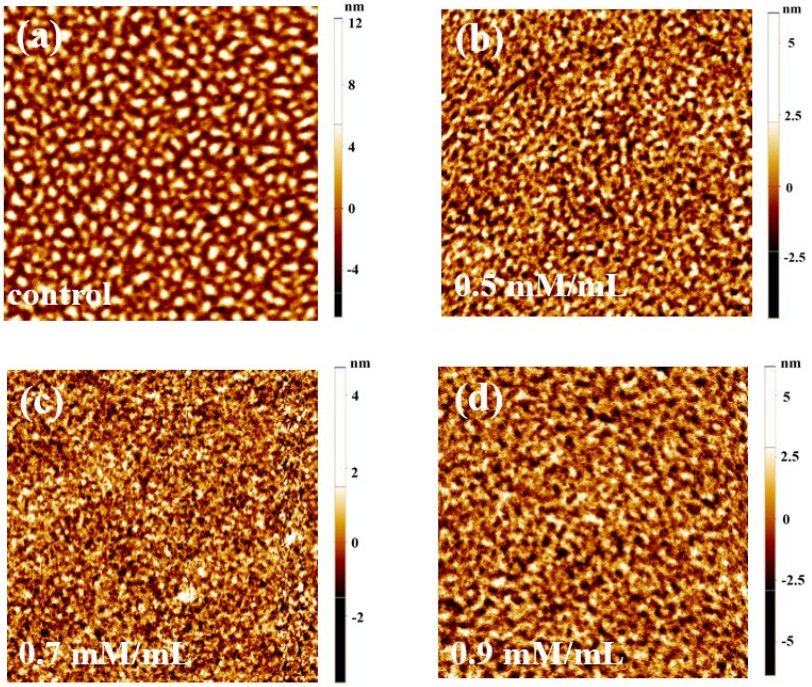

Fig. S1 AFM images of the quasi-2D perovskite film without and with different concentrations of AuAg-NPrisms@SiO_2 at the interface.

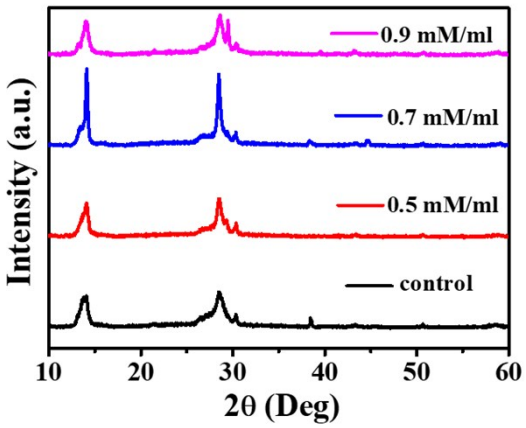

Fig. S2 XRD patterns of the quasi-2D perovskite film without and with different concentrations of AuAg-NPrisms@SiO_2 at the interface.

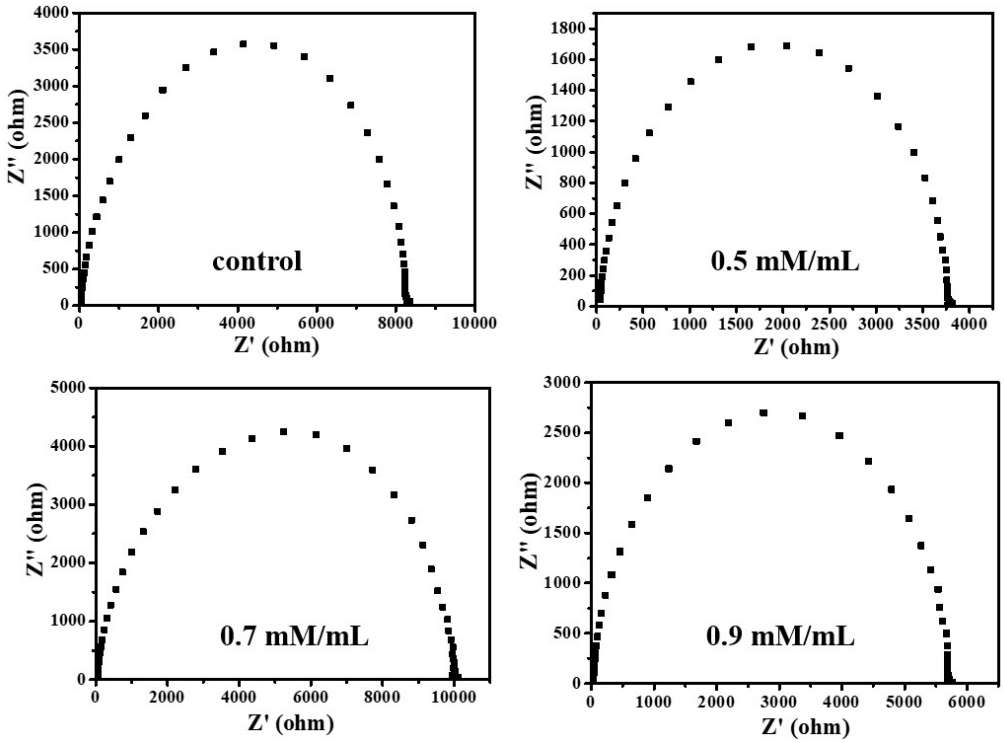

Fig. S3 EIS of the devices without and with 0.5, 0.7, 0.9 mM/mL AuAg-NPrisms@SiO_2.

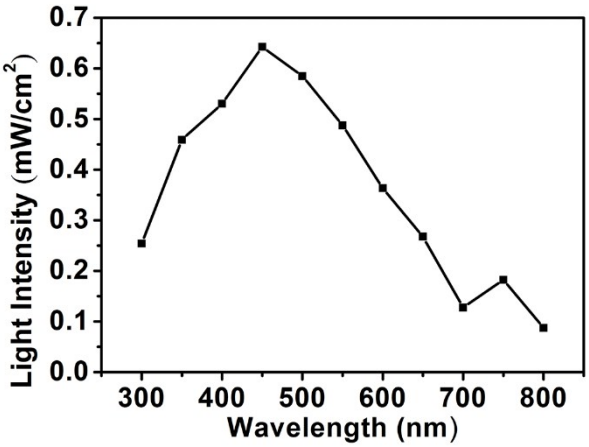

Fig. S4 Power densities of illuminations versus wavelength for the Xe lamp.

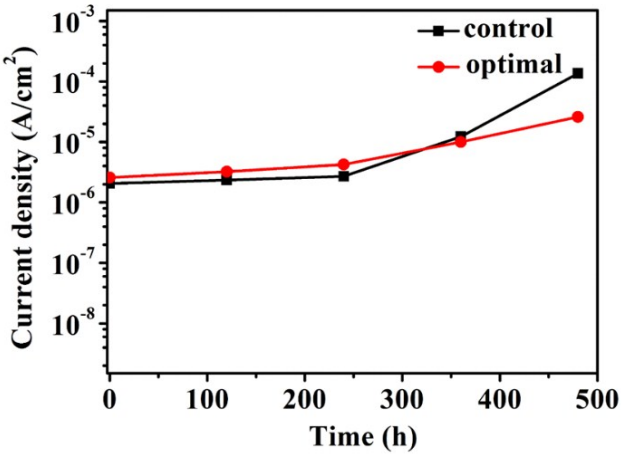

Fig. S5 Stability of the dark current of the control and optimal devices (under 35% relative humidity in an ambient environment without any encapsulation layer).

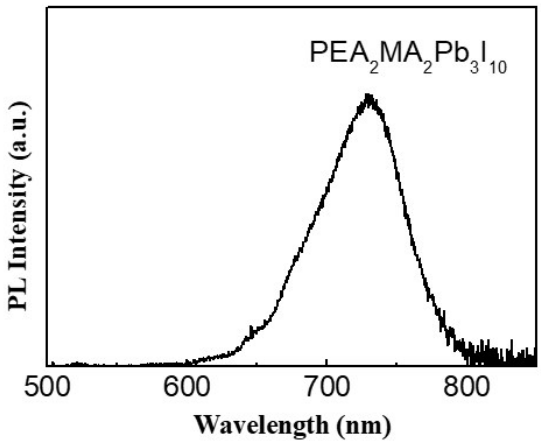

Fig. S6 Steady-state PL spectra of $(PEA)_2(MA)_2Pb_3I_{10}$ film on glass.

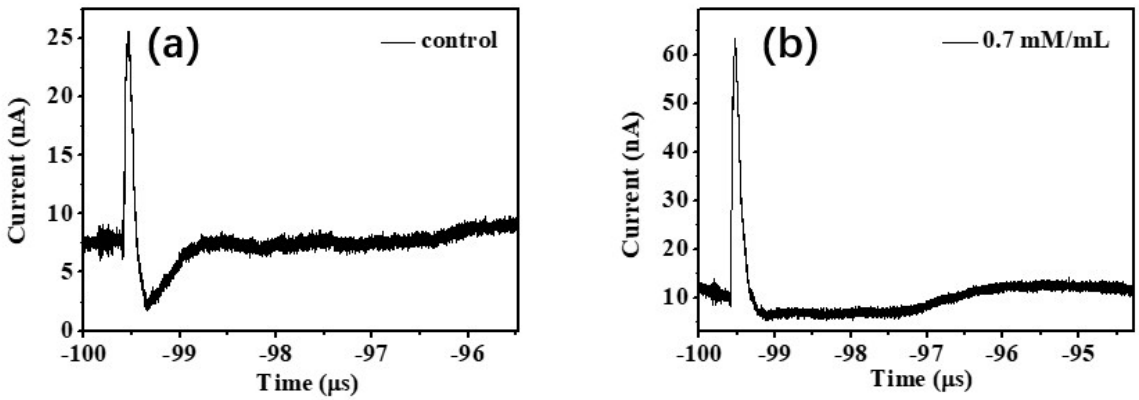

Fig. S7 Response speed of the control and optimal devices.

Table I Performances of 2D perovskite-based PDs

Active layer	I_{light} / I_{dark}	R	D*	Response time	Ref
$(C_6H_9C_2H_4NH_3)_2PbI_4$ films				>20 s	[3]
$(BA)_2PbBr_4$ crystals	10^3	2100 A/W			[4]
$(BA)_2(MA)_2Pb_3I_{10}$ (n = 3) films	10^3	12.78 mA/W		10 ms 7.5 ms	[5]
$(BA)_2(MA)_2Pb_3Br_{10}$ single crystal	2.5×10^3		3.6×10^{10} Jones	tr = 150 μs tf = 570 μs	[6]
$(BA)_2(MA)_{n-1}Pb_nI_{3n+1}$ nanowires (n = 4)		1.5×10^4 A /W	7×10^{15} Jones	tr = 27.6 μs tf = 24.5 μs	[7]
$(EMA)_2(MA)Pb_2I_7$ single crystal	$>10^3$	3.87 mA/ W	2.92×10^{10}Jones	tr = 1.52 μs tf = 1.67 μs	[8]
$(PEA)_2PbBr_4$ single crystal	10^3				[9]
$(BA)_2(MA)_{n-1}Pb_nX_{3n+1}$ n = 2, 3 single crystal	2862 n = 3	2.96 A/W n = 2	10^{13} Jones n = 2	<4 ms n = 2	[10]
$(BA)_2(MA)Pb_2I_7$ single crystal	10^3		10^{11} Jones	tr = 125 ms tf = 74 ms	[11]
$(BA)_2(MA)Pb_2Br_7$ crystals	1.2×10^3		1.1×10^9 Jones	tr = 20 μs tf = 28 μs	[12]
$(PEA)_2PbI_4$ single crystal		139.6 A/W	1.89×10^{15} Jones	tr = 21 μs tf = 37 μs	[13]
$(HFA)_2(FA)Pb_2I_7$ crystals	10^3	0.95 mA/w	3×10^{11} Jones	tr = 310 μs tf = 520 μs	[14]
$(PEA)_2PbBr_4$ single crystal	10^5	31.48 mA /W	1.55×10^{13} Jones	0.4 ms	[15]
$(PEA)_2(MA)_2Pb_3I_{10}$ films	10^3	7.15 A/W	3.2×10^{13} Jones	tr = 29 ns tf = 152 ns	Our results

[1] W. Wang, Y. Cui, K. H. Fung, Y. Zhang, T. Ji, and Y. Hao, Comparison of Nanohole-Type and Nanopillar-Type Patterned Metallic Electrodes Incorporated in Organic Solar Cells, Nanoscale Res. Lett. **12**(1) (2017).

[2] Z. Wang, Y. Hao, W. Wang, Y. Cui, Q. Sun, T. Ji, Z. Li, H. Wang, and F. R. Zhu, Incorporating silver-SiO_2 core-shell nanocubes for simultaneous broadband absorption and charge collection enhancements in organic solar cells, Synthetic Met. **220** (2016) 612-620.

[3] S. Ahmad, P. K. Kanaujia, H. J. Beeson, A. Abate, F. Deschler, D. Credgington, U. Steiner, G. V. Prakash and J. J. Baumberg, ACS Appl Mater Interfaces, 2015, 7, 25227.

[4] Z. Tan, Y. Wu, H. Hong, J. Yin, J. Zhang, L. Lin, M. Wang, X. Sun, L. Sun, Y. Huang, K. Liu, Z. Liu and H. Peng, J Am Chem Soc, 2016, 138, 16612.

[5] J. Zhou, Y. Chu and J. Huang, ACS Appl Mater Interfaces, 2016, 8, 25660.

[6] L. Li, Z. Sun, P. Wang, W. Hu, S. Wang, C. Ji, M. Hong and J. Luo, Angew Chem Int Ed Engl, 2017, 56, 12150.

[7] J. Feng, C. Gong, H. Gao, W. Wen, Y. Gong, X. Jiang, B. Zhang, Y. Wu, Y. Wu, H. Fu, L. Jiang and X. Zhang, Nature Electronics, 2018, 1, 404.

[8] S. Han, P. Wang, J. Zhang, X. Liu, Z. Sun, X. Huang, L. Li, C. Ji, W. Zhang, B. Teng, W. Hu, M. Hong and J. Luo, Laser & Photonics Reviews, 2018, 12, 1800060.

[9] C. Ge, W. Zhai, C. Tian, S. Zhao, T. Guo, S. Sun, W. Chen and G. Ran, RSC Advances, 2019, 9, 16779.

[10] X. He, Y. Wang, K. Li, X. Wang, P. Liu, Y. Yang, Q. Liao, T. Zhai, J. Yao and H. Fu, ACS Appl Mater Interfaces, 2019, 11, 15905.

[11] J. Li, J. Wang, J. Ma, H. Shen, L. Li, X. Duan and D. Li, Nature Communications, 2019, 10, 806.

[12] L. Li, X. Liu, Y. Li, Z. Xu, Z. Wu, S. Han, K. Tao, M. Hong, J. Luo and Z. Sun, Journal of the American Chemical Society, 2019, 141, 2623.

[13] Y. Liu, H. Ye, Y. Zhang, K. Zhao, Z. Yang, Y. Yuan, H. Wu, G. Zhao, Z. Yang, J. Tang, Z. Xu and S. Liu, Matter, 2019, 04, 002.

[14] Y. Wang, X. Liu, L. Li, C. Ji, Z. Sun, S. Han, K. Tao and J. Luo, Chemistry – An Asian Journal, 2019, 14, 1530.

[15] Y. Zhang, Y. Liu, Z. Xu, H. Ye, Q. Li, M. Hu, Z. Yang and S. Liu, J. Mater. Chem. C, 2019, 7, 1584.

